Applied Radiation and Isotopes 107 (2016) 206–213

Contents lists available at ScienceDirect

Applied Radiation and Isotopes

journal homepage: www.elsevier.com/locate/apradiso

Modeling the transmission of beta rays through thin foils in planar geometry

D. Stanga [a,*], P. De Felice [b], J. Keightley [c], M. Capogni [b], E. Ionescu [a]

[a] National Institute of R&D for Physics and Nuclear Engineering-HoriaHulubei, IFIN-HH, P.O. Box MG-6, Bucharest, Magurele, R-077125, Romania
[b] Instituto Nazionale di Metrologia delle Radiazioni Ionizzante, ENEA, C.R. Casaccia, P.O. Box 2400, I-00100 Rome, Italy
[c] National Physical Laboratory, Hampton Road, Teddington TW11 0LW, UK

HIGHLIGHTS

- A mathematical model of electron transport in planar geometry is developed.
- The model is based on the plane source concept.
- The efficiency of plane sources is computed using Monte Carlo method.
- A simple function for the plane source efficiency is obtained by curve fitting.
- Applications of the mathematical model are also presented.

ARTICLE INFO

Article history:
Received 16 January 2015
Received in revised form
19 October 2015
Accepted 20 October 2015
Available online 23 October 2015

Keywords:
Modeling
Beta-rays
Transmission
Planar geometry

ABSTRACT

This paper is concerned with the modeling of the transmission of beta rays through thin foils in planar geometry based on the plane source concept, using Monte Carlo simulation of electron transport and least squares fitting. Applications of modeling results for calculating the efficiency of large-area beta sources, transmission coefficient of beta rays through thin foils and the beta detection efficiency of large-area detectors used in surface contamination measurements are also presented.

1. Introduction

The transmission of beta rays through thin absorbers in planar geometry is quite different from the case of collimated beams. This is due to the fact that the emission of beta particles is isotropic and the majority of trajectories through the absorber are longer than the thickness of the absorber. The geometry effect on experimentally determined transmission curves (Jansen and Klein, 1996) and a heuristic approach for calculating roughly the attenuation of beta-rays in thin absorbers in planar geometry have already been reported (Haemers et al., 2007). Monte Carlo simulation of the electron transport through thin foils in planar geometry was also performed for determining the efficiency of large-area beta sources (Berger, 1998; Svec et al., 2006; Stanga et al., 2011).

The mathematical modeling of the transmission of beta rays through thin foils in planar geometry is useful for a range of applications such as standardization of large-area sources (ISO, 2010; Berger et al., 1996), calibration of contamination monitors (IEC, 2002), evaluation of surface contamination (ISO, 1988; ISO, 1996) and gross beta counting (ISO, 1992; Pujol and Suarez-Navarro, 2004). By mathematical modeling, the problems from these areas are translated into tractable mathematical formulations whose theoretical and numerical analysis provides insight, answers and guidance useful for these applications.

This paper deals mainly with the modeling of the transmission of beta-rays through thin foils in planar geometry based on the plane source concept (Berger et al., 1996), using Monte Carlo simulation of electron transport and least squares fitting. Thus, the efficiency of plane sources located at different source depths was computed by Monte Carlo method and Monte Carlo data were fitted by the linear least squares method with a polynomial function which depends on the square root of the source depth.

As a result of modeling, mathematical tools were developed for calculating the efficiency of large-area beta emitting sources, the

* Corresponding author.
E-mail address: doru@nipne.ro (D. Stanga).

http://dx.doi.org/10.1016/j.apradiso.2015.10.024
0969-8043/

transmission coefficient of beta rays through thin foils and the beta detection efficiency of large-area counters. These are powerful tools with many applications in the areas mentioned above. Thus, the integral equation for calculating the source efficiency provides a simple relationship between the surface emission rate and the activity of large-area beta emitting sources. This is in contrast with the general opinion that there is not a simple and known relationship between these quantities (ISO, 2010). The same integral equation can be used for evaluating the surface contamination by calculating the efficiency of beta contamination sources. The standard ISO 7503-1 provides two suggested default values for the efficiency of beta contamination sources but they do not have a strong theoretical basis (ISO, 1988).

Novel methods of measurement can be developed by using the integral equations for calculating the source efficiency and the transmission coefficient. A new method, based on these equations, for determining the activity of large-area beta reference sources constructed from anodized aluminum foils has already been reported (Stanga, 2014). The integral equation for calculating the detection efficiency can be used for investigating under which conditions the calibration of surface contamination meters on the basis of activity per unit area is useful.

In September 2014 the three year duration Joint Research Project "MetroDecom-Metrology for decommissioning nuclear facilities" started in the frame of the European Metrology Research Programme (EMRP). One of specific objectives of the project is to improve the accuracy and traceability of surface beta contamination measurements. The modeling of the transmission of beta rays through thin foils in planar geometry is the starting point in the achievement of this objective.

2. Transmission of beta-rays emitted by plane sources through thin foils

2.1. Efficiency of plane sources

We consider the large-area source shown in Fig. 1 without the covering foil. In this planar geometry the source substratum of thickness Δ is placed on a backing plate both being constructed from the same material of circular shape having identical radii. The activity is incorporated into the top surface of the source substratum resulting in a source which has a thin active layer and a circular shape. The backing plate is thick and the radius of the active layer is small to prevent emission of the beta radiation through the back and the side of the source. We used a circular type source but the results of this paper remain valid for any type of planar source.

For a point source of infinitesimal volume assumed to be located at the position (x, y, z), its emission rate in 2π, $E(x, y, z)dxdydz$, is defined as the rate of beta particles that emerge from the top surface of the large-area source in a 2π solid angle. The emission in 2π of the source results from the interplay of two factors. On the one hand, emission is increased due to the backscattering of beta particles by the backing plate, while on the other hand, the emission is decreased due to the absorption of beta particles by the substratum material. The efficiency of the point source is defined as the ratio between its emission rate $E(x, y, z)dxdydz$ and its activity $\Lambda(x, y, z)dxdydz$ (assuming that the emission probability of beta particles is 100%). It is evident that the efficiency of the point source does not depend on the coordinates y and z. Under these conditions, the efficiency, $\varepsilon_p(x)$, of the plane source located at the depth x can be defined as

$$\varepsilon_p(x) = \frac{E_p(x)}{\Lambda_p(x)} \tag{1}$$

where $\Lambda_p(x) = \iint_S \Lambda(x, y, z)dydz$, $E_p(x) = \iint_S E(x, y, z)dydz$ (S is the surface of the plane source), $\Lambda_p(x)dx$ and $E_p(x)dx$ represent the activity and the emission rate in 2π of the plane source. In case that the substratum material is different from the material of the backing plate, $\varepsilon_p(x, \Delta)$ depends on both x and the thickness Δ of the substratum material. This is due to the fact that the electrons are backscattered by a double-layered material composed of a backing plate (with the thickness higher than the backscattering saturation thickness) and a thin layer of variable thickness containing the substratum material (see chapter 3). In this case, Eq. (1) becomes

$$\varepsilon_p(x, \Delta) = \frac{E_p(x, \Delta)}{\Lambda_p(x)} \tag{2}$$

In practice, large-area beta sources are often constructed as it is shown in Fig. 2. This planar geometry is equivalent with the geometry from Fig. 1 when the substratum and backing plate are made from the same material. In case that these materials are different, the efficiency of a point source located at the position (x, y, z) depends on the coordinates y and z located near the source edge. Consequently, the efficiency of the plane source from the depth x depends on the coordinates y and z. However, this edge effect can be neglected if the atomic numbers of materials are close and/or the source radius is much longer than the maximum range of beta-rays in the substratum material.

As mentioned above, Eq. (1) is valid for nuclides that emit beta radiations with emission probability of 100% such as ^{14}C, ^{147}Pm, ^{60}Co, ^{36}Cl and ^{90}Sr–^{90}Y. In case of nuclides that emit both beta particles having a continuous energy spectrum and conversion electrons having discrete energies E_i with emission probabilities f_i (i=1, 2,…,n), the plane source efficiency can be written as

$$\varepsilon_p(x) = \frac{E_p(x)}{f_T \cdot \Lambda_p(x)} = \frac{E_b(x) + E_{ce}(x)}{f_T \Lambda_p(x)} = \frac{f_b \varepsilon_{pb}(x) + f_{ce} \varepsilon_{pce}(x)}{f_T} \tag{3}$$

where $E_b(x)$, f_b and $\varepsilon_{pb}(x)$ are, respectively, the emission rate in 2π, the emission probability and the plane source efficiency corresponding to beta particles, $E_{ce}(x)$, f_{ce} and $\varepsilon_{pce}(x)$ are, respectively, the emission rate in 2π, the total emission probability and the plane source efficiency corresponding to conversion electrons, $f_T = f_b + f_{ce}$ and $E_p(x) = E_b(x) + E_{ce}(x)$. It should be noted that Eq. (3) reduces to Eq. (1) when f_b=1 and f_{ce}=0. The efficiency, $\varepsilon_{ce}(x)$, is given by

$$\varepsilon_{ce}(x) = \frac{E_{ce}(x)}{f_{ce}\Lambda_p(x)} = \frac{1}{f_{ce}} \sum_{i=1}^{n} f_i \varepsilon_{pi}(x) \tag{4}$$

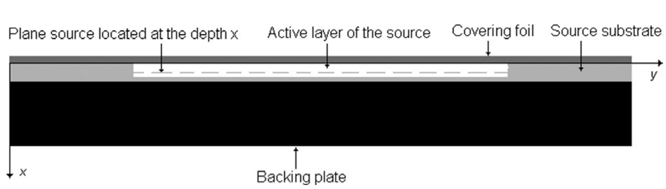

Fig. 1. Schematic view of a large-area source covered by a thin foil.

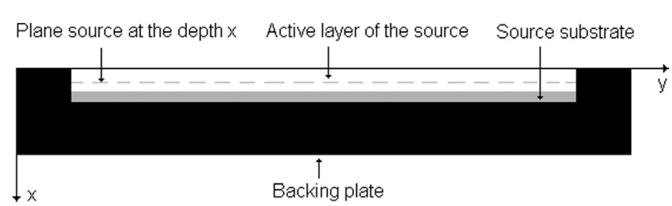

Fig. 2. Schematic view of a new type of large-area source.

where $f_{ce} = \sum_{i=1}^{n} f_i$and $\varepsilon_{pi}(x)$ is the plane source efficiency corresponding to conversion electrons of energy E_i. The radionuclide ^{137}Cs is an example of nuclide that emits both beta radiations and conversion electrons (via ^{137m}Ba metastable state with $T_{1/2}$ =2.55 min). These electrons have three discrete energies E_1=624 keV, E_2=656 keV and E_3=660 keV with emission probabilities f_1=0.0762, f_2=0.0142 and f_3=0.0033 (Bé et al., 2006; Yunoki et al., 2013).

Taking into account the covering foil of thickness s shown in Fig. 1, the efficiency of the plane source located at the depth x, $\varepsilon_{ps}(x, \Delta, s)$, can be defined as

$$\varepsilon_{ps}(x, \Delta, s) = \frac{E_{ps}(x, \Delta, s)}{f_T \cdot \Lambda_p(x)} \tag{5}$$

where the emission rate in 2π of the plane source (the rate of beta particles that emerge from the top surface of the covering foil in a 2π solid angle), $E_{ps}(x, \Delta, s)$, depends on x, Δ and s. The transmission coefficient of beta rays emitted by the plane source through the foil of thickness s is defined as

$$t_p(x, \Delta, s) = \frac{E_{ps}(x, \Delta, s)}{E_p(x, \Delta)} = \frac{\varepsilon_{ps}(x, \Delta, s)}{\varepsilon_{ps}(x, \Delta)} \tag{6}$$

and represents the fraction of beta particles transmitted through this foil.

The concept of plane source, introduced by Berger et al. (1996), is useful in treating the efficiency of large-area beta sources and the transmission of beta rays through thin foils in planar geometry because the plane source efficiency can easily be calculated by Monte Carlo method and depends only on the source depth x and the thickness, Δ, of the source substrate.

2.2. Computing the efficiency of plane sources by Monte Carlo method

Electron transport calculations by the Monte Carlo method were carried out using the Pencyl code from the simulation package PENELOPE (Baro et al., 1995). This code simulates electron–photon showers in multilayered cylindrical structures. The reliability of the simulation package PENELOPE for simulating the electron transport was confirmed in different benchmark comparisons and comparative studies (Sempau et al., 2003; Vilches et al., 2007). In the Pencyl code, the simulation of electron tracks is performed by means of a mixed (class II) algorithm. A detailed description of cross sections and simulation methods adopted in

Table 1
Values of $\varepsilon_p(x)$computed by Monte Carlo method for five nuclides and different values x of the source depth using aluminum and Mylar as materials for both the backing plate and the source substrate.

Backing plate: aluminum Source substrate: aluminum									
^{14}C		^{147}Pm		^{60}Co		^{36}Cl		^{90}Sr-^{90}Y	
x (mg/cm2)	$\varepsilon_p(x)$	x (mg/cm2)	$\varepsilon_p(x)$	x (mg/cm2)	$\varepsilon_p(x)$	x (mg/cm2)	$\varepsilon_p(x)$	x (mg/cm2)	$\varepsilon_p(x)$
0.000	0.7205	0.000	0.7192	0.000	0.7174	0.000	0.7147	0.000	0.7100
0.027	0.6345	0.027	0.6372	0.027	0.6648	0.135	0.6732	0.135	0.6740
0.054	0.5993	0.054	0.6056	0.054	0.6432	0.270	0.6553	0.270	0.6596
0.081	0.5735	0.135	0.5487	0.135	0.6032	0.540	0.6320	0.540	0.6394
0.135	0.5342	0.216	0.5112	0.270	0.5608	1.080	0.5960	1.080	0.6125
0.216	0.4906	0.270	0.4912	0.405	0.5305	1.620	0.5710	1.620	0.5935
0.270	0.4669	0.405	0.4510	0.540	0.5065	2.160	0.5478	2.160	0.5775
0.405	0.4202	0.540	0.4198	0.810	0.4676	2.700	0.5298	2.700	0.5620
0.540	0.3830	0.675	0.3942	1.080	0.4370	3.510	0.5055	3.510	0.5438
0.810	0.3270	0.810	0.3715	1.350	0.4114	5.400	0.4595	5.400	0.5100
1.080	0.2843	1.080	0.3346	1.620	0.3894	7.560	0.4165	7.560	0.4783
1.620	0.2222	1.620	0.2797	2.160	0.3517	9.180	0.3899	10.80	0.4412
2.160	0.1781	2.160	0.2392	2.700	0.3216	10.800	0.3661	16.20	0.3946
2.700	0.1456	2.700	0.2078	3.240	0.2951	13.500	0.3317	21.60	0.3585
3.240	0.1199	3.240	0.1821	4.320	0.2531	16.200	0.3020	32.40	0.3048
3.780	0.0994	3.780	0.1610	5.400	0.2200	21.600	0.2528	43.20	0.2659
4.320	0.0831	4.320	0.1430	6.750	0.1866	27.000	0.2136	54.00	0.2364
4.860	0.0696	5.400	0.1138	8.100	0.1598	35.100	0.1680	70.20	0.2034
5.400	0.0585	6.750	0.0875	10.80	0.1190	43.200	0.1327	94.50	0.1686
6.750	0.0382	8.100	0.0679	13.50	0.0900	54.000	0.0971	162.0	0.1123
Backing plate: mylar Source substrate: mylar									
0.000	0.6700	0.000	0.6700	0.000	0.6680	0.000	0.6660	0.000	0.6630
0.007	0.6293	0.007	0.6298	0.035	0.6122	0.070	0.6381	0.070	0.6400
0.014	0.6110	0.014	0.6130	0.070	0.5900	0.140	0.6270	0.140	0.6310
0.035	0.5781	0.035	0.5830	0.105	0.5727	0.280	0.6098	0.280	0.6160
0.070	0.5420	0.070	0.5500	0.140	0.5600	0.420	0.5974	0.700	0.5911
0.105	0.5153	0.105	0.5269	0.210	0.5377	0.700	0.5780	1.400	0.5630
0.140	0.4940	0.140	0.5090	0.280	0.5206	1.400	0.5430	2.100	0.5430
0.175	0.4757	0.210	0.4787	0.350	0.5060	2.100	0.5165	2.800	0.5260
0.210	0.4594	0.280	0.4549	0.420	0.4924	2.800	0.4940	4.200	0.4992
0.280	0.4320	0.350	0.4350	0.700	0.4510	4.200	0.4581	7.000	0.4590
0.420	0.3881	0.420	0.4179	1.050	0.4124	5.600	0.4290	14.000	0.3910
0.560	0.3542	0.700	0.3650	1.400	0.3820	7.000	0.4034	21.000	0.3454
0.700	0.3256	0.840	0.3437	1.750	0.3564	8.400	0.3808	28.000	0.3100
0.840	0.3013	0.980	0.3258	2.100	0.3350	9.800	0.3610	35.000	0.2817
0.980	0.2810	1.400	0.2820	2.800	0.2983	14.000	0.3110	42.000	0.2590
1.400	0.2310	2.100	0.2300	3.500	0.2690	21.000	0.2480	56.000	0.2230
2.100	0.1730	2.800	0.1920	4.900	0.2230	28.000	0.2007	70.000	0.1962
2.800	0.1330	4.200	0.1400	7.000	0.1731	35.000	0.1640	84.000	0.1760
3.500	0.1045	4.900	0.1207	9.800	0.1280	49.000	0.1105	112.000	0.1460
4.200	0.0830	5.600	0.1050	12.600	0.0956	52.500	0.1003	154.000	0.1150

Table 2
Values of $\varepsilon_{pb}(x)$, $\varepsilon_{p1}(x)$, $\varepsilon_{p2}(x)$ and $\varepsilon_{p3}(x)$ for ^{137}Cs plane sources computed by Monte Carlo method for different values x of the source depth using aluminum and Mylar as materials for both the backing plate and the source substrate.

x (mg/cm^2)	$\varepsilon_{pb}(x)$	x (mg/cm^2)	$\varepsilon_{pb}(x)$	x (mg/cm^2)	$\varepsilon_{p1}(x)$	$\varepsilon_{p2}(x)$	$\varepsilon_{p3}(x)$
Backing plate: aluminum Source substrate: aluminum							
0.000	0.71500	5.400	0.37500	0.000	0.7080	0.7080	0.7080
0.135	0.64750	6.480	0.35110	0.675	0.6910	0.6910	0.6912
0.270	0.62300	7.560	0.32900	1.350	0.6820	0.6830	0.6830
0.540	0.58710	9.180	0.30170	2.700	0.6680	0.6700	0.6701
1.080	0.54000	10.80	0.27700	6.750	0.6371	0.6400	0.6410
1.620	0.50750	13.50	0.24330	13.500	0.5960	0.6021	0.6026
2.160	0.48100	16.20	0.21460	20.250	0.5610	0.5680	0.5683
2.700	0.45700	21.60	0.17040	27.000	0.5282	0.5370	0.5380
3.510	0.42790	27.00	0.13660	33.750	0.4990	0.5092	0.5100
4.320	0.40400	37.80	0.08935	40.500	0.4690	0.4810	0.4830
Backing plate: Mylar Source substrate: Mylar							
0.000	0.6660	2.800	0.4260	0.000	0.6636	0.6633	0.6632
0.035	0.6337	4.200	0.3835	0.350	0.6528	0.6527	0.6530
0.070	0.6201	5.600	0.3500	0.700	0.6469	0.6478	0.6476
0.140	0.6030	7.000	0.3227	1.400	0.6393	0.6398	0.6394
0.210	0.5889	10.500	0.2702	3.500	0.6204	0.6221	0.6215
0.350	0.5690	14.000	0.2280	7.000	0.5973	0.5998	0.5999
0.700	0.5330	17.500	0.1951	14.000	0.5601	0.5645	0.5653
1.050	0.5069	21.000	0.1690	21.000	0.5277	0.5337	0.5355
1.400	0.4860	28.000	0.1280	28.000	0.4981	0.5063	0.5068
2.100	0.4526	35.000	0.0970	42.000	0.4437	0.4543	0.4547

PENELOPE is given by Salvat et al. (2003). The Pencyl code can also perform a purely detailed simulation (collision by collision). Mixed simulation is faster than detailed simulation but detailed simulation usually provides more accurate results that are only affected by statistical uncertainties and inaccuracies of the physical interaction model. Both the mixed simulation and the detailed simulation were used to compute the efficiency of plane sources and the results were practically the same.

Electron transport calculations were first carried out for the planar geometry shown in Fig. 1 using the same material for the backing plate and the source. Table 1 shows the values of $\varepsilon_p(x)$ computed by Pencyl code for different values of x and a set of five beta emitters ^{14}C, ^{147}Pm, ^{60}Co, ^{36}Cl, ^{90}Sr–^{90}Y. Table 2 shows the values of $\varepsilon_{pb}(x)$, $\varepsilon_{p1}(x)$, $\varepsilon_{p2}(x)$ and $\varepsilon_{p3}(x)$ in the case of ^{137}Cs plane sources for different values of x. Aluminum and Mylar were used for both the backing plate and the substrate. All Monte Carlo data were computed with relative standard uncertainties smaller than 0.3%.

Electron transport calculations were also carried out for determining the efficiency of ^{36}Cl plane sources using aluminum as material for the backing plate and Mylar as source substrate. In Table 3 are shown the values of $\varepsilon_p(x, \Delta)$ for different values of x computed for $\Delta = 15.6$ mg/cm^2.

Table 3
Values of $\varepsilon_p(x, \Delta)$computed by Monte Carlo method for ^{36}Cl plane sources, different values x of the source depth and $\Delta = 15.6$ mg/cm^2 using aluminum as material for the backing plate and Mylar as material for the source substrate.

x (mg/cm^2)	$\varepsilon_p(x, \Delta)$	x (mg/cm^2)	$\varepsilon_p(x, \Delta)$
0.00	0.6787	2.10	0.5305
0.07	0.6507	3.50	0.4905
0.14	0.6392	4.90	0.4595
0.28	0.6229	7.00	0.4212
0.56	0.6005	9.80	0.3816
0.84	0.5834	12.60	0.3499
1.40	0.5568	15.60	0.3246

2.3. *Least square fitting of Monte Carlo data*

The Monte Carlo data were fitted with deviations of less than 0.5% by the following polynomial function in the variable square root of x.

$$\varepsilon_p(x) = a_0 + a_1 x^{0.5} + a_2 x^{1.0} + a_3 x^{1.5} + a_4 x^{2.0} + a_5 x^{2.5} \tag{7}$$

where a_0, a_1, a_2, a_3, a_4 and a_5 are fitting parameters. In Table 4 are shown the values of fitting parameters for ^{14}C, ^{147}Pm, ^{60}Co, ^{36}Cl, and ^{90}Sr–^{90}Y plane sources which were computed using Monte Carlo data from Table 1. One can see from Table 4 that $\varepsilon_p(x)$ depends not only on x but also on materials used for the backing plate and the source substrate. It is also evident that $a_0 = (1+\eta_S)/2$ where η_S is the saturation backscattering coefficient of the backing plate material (see chapter 3).

In the case of ^{137}Cs plane sources, the fitting parameters, $a_i (i=0, 1, 2, 3, 4, 5)$, were calculated by means of Eq. (3) as follows

$$a_i = \frac{f_b a_{ib} + f_1 a_{i1} + f_2 a_{i2} + f_3 a_{i3}}{f_T} \tag{8}$$

where a_{ib}, a_{i1}, a_{i2}, a_{i3} are, respectively, the fitting parameters corresponding to $\varepsilon_{pb}(x)$, $\varepsilon_{p1}(x)$, $\varepsilon_{p2}(x)$, $\varepsilon_{p3}(x)$. These parameters were computed using Monte Carlo data from Table 2. Table 5 shows the parameters $a_i$which were calculated by means of Eq. (8). In Fig. 3 is shown $\varepsilon_p(x)$ for ^{14}C, ^{147}Pm, ^{60}Co, ^{137}Cs, ^{36}Cl and ^{90}Sr–^{90}Y plane sources and $x \in [0, 7]$ mg/cm^2 using aluminum as material for both backing plate and source substrate.

Monte Carlo data from Table 3 were also fitted with the function expressed by Eq. (7). The following values of the fitting parameters were obtained: $a_0 =$ 0.67866, $a_1 = -0.10582$, $a_2 =$ 0.00017, $a_3 =$ 0.00261, $a_4 = -0.00083$ and $a_5 =$ 0.00011. As one can see, $a_0 = (1 + \eta_S^{(am)}(\Delta))/2$ where $\eta_S^{(am)}(\Delta)$ is the backscattering coefficient at saturation of the double-layered material composed of the aluminum plate and the Mylar substrate of thickness $\Delta = 15.6$ mg/cm^2 (see Eq. (11)).

3. Backscattering of beta-rays in planar geometry

The backscattering coefficient is defined as the ratio of the number of backscattered beta particles to the number of beta

Table 4
Values of the parameters a_0, a_1, a_2, a_3, a_4 and a_5 obtained by least squares fitting of Monte Carlo data from Table 1.

Parameters	^{14}C	^{147}Pm	^{60}Co	^{36}Cl	^{90}Sr–^{90}Y
Backing plate: aluminum Source substrate: aluminum					
a_0	0.721095409	0.719180278	0.717789557	0.715109231	0.709496911
a_1 (cm/mg$^{0.5}$)	−0.554508690	−0.534596470	−0.340266940	−0.115271820	−0.098614630
a_2 (cm^2/mg)	0.121308877	0.218489073	0.084607399	0.000130448	0.005957814
a_3 (cm^3/mg$^{1.5}$)	0.019860022	−0.073902140	−0.020256230	0.001071889	−0.000304160
a_4 (cm^4/mg^2)	−0.014401100	0.017351480	0.003832716	−0.000094503	0.000024287
a_5 (cm^5/mg$^{2.5}$)	0.002085874	−0.001790780	−0.000318940	0.000003376	−0.000000950
Backing plate: Mylar Source substrate: Mylar					
a_0	0.670716345	0.670142842	0.668312343	0.666195460	0.663283958
a_1 (cm/mg$^{0.5}$)	−0.519479640	−0.507823940	−0.320046400	−0.107256370	−0.090951850
a_2 (cm^2/mg)	0.122417795	0.237092755	0.090804341	0.002131739	0.006006713
a_3 (cm^3/mg$^{1.5}$)	0.021748840	−0.102182100	−0.027440120	0.000364491	−0.000416620
a_4 (cm^4/mg^2)	−0.021923850	0.030166282	0.006049652	−0.000015832	0.000034107
a_5 (cm^5/mg$^{2.5}$)	0.004492794	−0.003815360	−0.000557110	0.000000217	−0.000001214

particles hitting the surface of the backing plate. The backscattering coefficient increases with increasing backing plate thickness until saturation is reached. The largest backing layer, at which the backscattering coefficient reaches its maximal value, is called the thickness of saturation. The backscattering coefficient corresponding to values of the backing plate thickness higher than the saturation thickness is called saturation backscattering coefficient.

The backscattering coefficient in planar geometry was computed by means of the Pencyl code. Table 6 shows the values of the backscattering coefficient, $\eta(x)$, for different values, x, of the backing plate (aluminum) thickness. In the same table are also shown approximate values for the backscattering saturation thickness. An empirical model of $\eta(x)$ was obtained by least square fitting of data from Table 6 with the following function

$$\eta(x) = \frac{\alpha\sqrt{x}}{1 + \beta\sqrt{x}} \tag{9}$$

The values of fitting parameters α and β corresponding to ^{14}C, ^{147}Pm, ^{60}Co, ^{137}Cs, ^{36}Cl, and ^{90}Sr–^{90}Y are shown in Table 7.

The backscattering coefficient at saturation is of practical interest and therefore it was calculated for different materials of the backing plate using Pencyl code. In Table 8 are given the values of the saturation backscattering coefficient in planar geometry for ^{14}C, ^{147}Pm, ^{60}Co, ^{137}Cs, ^{36}Cl, ^{90}Sr–^{90}Y nuclides and for beryllium, carbon, aluminum, titanium, iron, molybdenum and tungsten materials. One can see from Table 8 that, for a given material, the saturation backscattering coefficient is almost constant for all nuclides. Its dependence on the atomic number Z can be approximated within 3% by the following relationship

$$\eta_S(Z) = 0.137\ \ln(Z) + 0.085 \tag{10}$$

The backscattering coefficient at saturation was also calculated for a double-layered material composed of an aluminum plate (with the thickness higher than the backscattering saturation thickness) and a Mylar foil. Results are shown in Table 9 for different values, x, of the Mylar foil thickness. An empirical model of the saturation backscattering coefficient, $\eta_S^{(am)}(x)$, was obtained by least square fitting of data from Table 9 with the following function

$$\eta_S^{(am)}(x) = \eta_S^{(my)} + (\eta_S^{(al)} - \eta_S^{(my)})\exp(-x/\theta) \tag{11}$$

where $\eta_S^{(al)}$ and $\eta_S^{(my)}$ are, respectively, the saturation backscattering coefficient of the aluminum plate and the Mylar foil and θ is the fitting parameter which is also shown in Table 9.

4. Comparison with data found in the literature

To check the validity of the models presented in this paper, we compare the Monte Carlo data obtained from Pencyl code with data from literature. Thus, the results reported by Berger in Table 2 of the paper (Berger, 1998) are compared with the Monte Carlo results given in Table 1 (aluminum) of this paper. The maximum discrepancy between results is 3.3% obtained in the case of the nuclide ^{14}C for x=2.16 mg/cm^2. Although the TRANSIT code used by Berger and Pencyl code have different interaction models and tracking algorithms, they give results in very good agreement.

In the paper (Seliger, 1952), the backscattering coefficient at saturation was measured in planar geometry (2π solid angle) for different materials of the backing plate (Lucite, aluminum, copper, silver and lead) using a 4π beta counter and a ^{32}P source (E_{max} =1.71 MeV). Discrepancies smaller than 10% were found between the results reported by Seliger in Fig. 2 of the paper (Selinger, 1952) and the results obtained in this work using Eq. (10). These discrepancies are due to the errors of calculation given by Eq. (10) and the uncertainty in the measurement of the saturation backscattering coefficient.

Though the reliability of the Pencyl code for electron transport was previously mentioned, the above comparisons give more confidence in the results obtained in this paper.

5. Applications

5.1. Efficiency of large-area beta sources

The surface emission rate, E_S, of the large-area source shown in Fig. 1 (covering foil is neglected) is defined by ISO 8769 and can be calculated by means of Eq. (2). Thus, we get

Table 5
Values of the parameters a_0, a_1, a_2, a_3, a_4, a_5 for ^{137}Cs plane sources obtained by means of Eq. (8).

Materials	a_0	a_1 (cm/mg$^{0.5}$)	a_2 (cm^2/mg)	a_3 (cm^3/mg$^{1.5}$)	a_4 (cm^4/mg^2)	a_5 (cm^5/mg$^{2.5}$)
Aluminum	0.714323109	−0.176106937	0.023339380	−0.003506495	0.000442019	−0.000023705
Mylar	0.665848407	−0.165421222	0.025099775	−0.004340524	0.000539681	−0.000027459

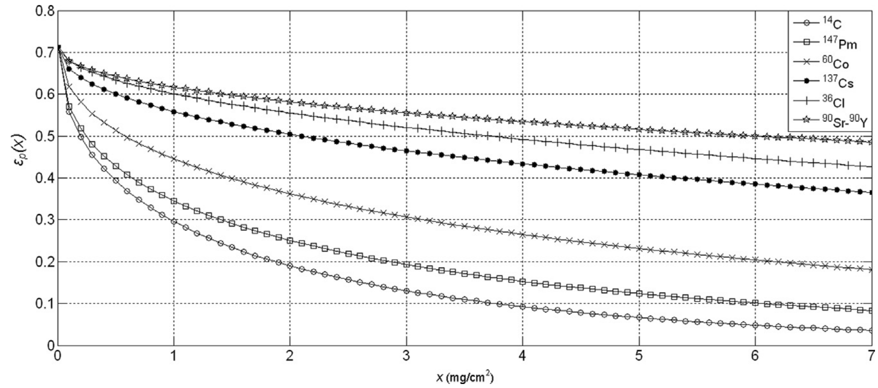

Fig. 3. The efficiency of ^{14}C, ^{147}Pm, ^{60}Co, ^{137}Cs, ^{36}Cl and ^{90}Sr–^{90}Y plane sources as a function of x. Using aluminum as material for both backing plate and source substrate.

$$E_S = f_T \int_0^{x_{\max}} \varepsilon_p(x, \Delta)\Lambda_p(x)dx = f_T\Lambda \int_0^{x_{\max}} \varepsilon_p(x, \Delta)f(x)dx \tag{12}$$

where Λ is the source activity, $f(x) = \Lambda_p(x)/\Lambda$ is the activity depth distribution and $x_{\max}$ represents the thickness of the active layer of the source which may be smaller than the thickness of the source material (see Fig. 1). Eq. (12) shows that there is a simple relationship between E_S and the activity, Λ, of the source and Λ can be calculated for a given value of E_S provided that $x_{\max}$ and $f(x)$ are known.

The efficiency, ε_S, of large-area beta sources is defined as the fraction of the emitted particles that emerge from the top surface of the source in a 2π solid angle. It follows that

$$\varepsilon_S = \frac{E_S}{f_T\Lambda} = \int_0^{x_{\max}} \varepsilon_p(x, \Delta)f(x)dx \tag{13}$$

In case that the same material is used for the backing plate and source substrate, $\varepsilon_p(x, \Delta)$ from Eqs. (12) and (13) must be replaced with $\varepsilon_p(x)$ (see Eq. (1)).

Taking into account that the source is covered by a foil of thickness s as it is shown in Fig. 1, the emission rate in 2π of the large-area source (the rate of beta particles emitted by the large-area source that emerge from the top surface of the covering foil in

Table 7
Values of the fitting parameters α and β for six radionuclides.

Parameters	^{14}C	^{147}Pm	^{60}Co	^{137}Cs	^{36}Cl	^{90}Sr–^{90}Y
α (cm/mg$^{0.5}$)	1.50	1.29	0.84	0.50	0.35	0.26
β (cm/mg$^{0.5}$)	2.96	2.53	1.64	1.01	0.68	0.56

Table 8
Values of the saturation backscattering coefficient for six nuclides and different materials as backing plates.

Backing plate	Z	Saturation backscattering coefficient					
		^{14}C	^{147}Pm	^{60}Co	^{137}Cs	^{36}Cl	^{90}Sr–^{90}Y
Beryllium	4	0.285	0.284	0.285	0.285	0.285	0.282
Carbon	6	0.333	0.332	0.331	0.330	0.329	0.324
Aluminum	13	0.440	0.438	0.436	0.430	0.430	0.420
Titanium	22	0.505	0.504	0.504	0.503	0.501	0.495
Iron	26	0.542	0.541	0.540	0.534	0.530	0.524
Molybdenum	42	0.603	0.603	0.604	0.604	0.603	0.592
Tungsten	74	0.677	0.677	0.684	0.689	0.690	0.679

Table 6
Values of the backscattering coefficient, *η(x)*, for aluminum computed by Monte Carlo method for six nuclides and different values *x* of the backing plate thickness together with approximate values of the backscattering saturation thickness.

^{14}C		^{147}Pm		^{60}Co		^{137}Cs		^{36}Cl		^{90}Sr – ^{90}Y	
x (mg/cm^2)	$\eta(x)$	x (mg/cm^2)	$\eta(x)$	x (mg/cm^2)	$\eta(x)$	x (mg/cm^2)	$\eta(x)$	x (mg/cm^2)	$\eta(x)$	x (mg/cm^2)	$\eta(x)$
0.000	0.000	0.000	0.000	0.000	0.000	0.000	0.000	0.000	0.000	0.000	0.000
0.027	0.161	0.027	0.156	0.054	0.148	0.135	0.139	0.135	0.110	0.540	0.138
0.054	0.206	0.054	0.190	0.135	0.192	0.270	0.167	0.270	0.136	1.080	0.169
0.135	0.264	0.135	0.242	0.216	0.218	0.540	0.203	0.540	0.166	1.620	0.190
0.216	0.296	0.216	0.272	0.270	0.228	1.080	0.244	1.080	0.204	2.160	0.205
0.270	0.304	0.270	0.286	0.540	0.270	1.620	0.270	2.160	0.247	2.700	0.218
0.405	0.332	0.405	0.306	0.810	0.298	2.160	0.289	2.700	0.263	4.320	0.246
0.540	0.352	0.540	0.324	1.080	0.316	2.700	0.304	3.510	0.282	5.400	0.259
0.810	0.378	0.810	0.350	1.620	0.344	3.510	0.320	4.320	0.296	7.560	0.280
1.080	0.394	1.080	0.368	2.160	0.362	4.320	0.336	5.400	0.313	10.80	0.302
1.620	0.412	1.620	0.390	2.700	0.374	5.400	0.350	7.560	0.337	16.20	0.326
2.160	0.424	2.160	0.404	3.240	0.386	7.560	0.371	10.80	0.363	21.60	0.342
2.700	0.430	2.700	0.414	4.320	0.400	9.180	0.382	16.20	0.388	37.80	0.369
3.240	0.434	3.240	0.420	6.750	0.418	10.80	0.391	21.60	0.402	54.00	0.384
3.780	0.436	3.780	0.424	8.100	0.424	16.20	0.410	32.40	0.418	81.00	0.398
5.400	0.440	4.320	0.426	10.80	0.430	21.60	0.419	37.80	0.422	135.0	0.412
6.750	0.444	6.750	0.436	13.50	0.434	32.40	0.428	48.60	0.428	216.0	0.420
8.100	0.444	8.100	0.436	16.20	0.434	35.10	0.428	51.30	0.428	230.0	0.420
Backscattering saturation thickness (mg/cm^2)											
^{14}C		^{147}Pm		^{60}Co		^{137}Cs		^{36}Cl		^{90}Sr–^{90}Y	
6.75		6.75		13.50		32.40		48.60		216.00	

Table 9
Values of the saturation backscattering coefficient, $\eta_S^{(am)}(x)$, corresponding to six nuclides and a two layered backing plate (aluminum-mylar), computed by Monte Carlo method for different values x of the Mylar foil thickness together with the values of the fitting parameter θ.

^{14}C		^{147}Pm		^{60}Co		^{137}Cs		^{36}Cl		^{90}Sr-^{90}Y	
x (mg/cm^2)	$\eta_S^{(am)}(x)$	x (mg/cm^2)	$\eta_S^{(am)}(x)$	x (mg/cm^2)	$\eta_S^{(am)}(x)$	x (mg/cm^2)	$\eta_S^{(am)}(x)$	x (mg/cm^2)	$\eta_S^{(am)}(x)$	x (mg/cm^2)	$\eta_S^{(am)}(x)$
0.00	0.444	0.00	0.438	0.00	0.436	0.00	0.430	0.00	0.429	0.00	0.420
0.14	0.412	0.28	0.404	0.56	0.404	0.70	0.410	1.40	0.410	7.00	0.384
0.28	0.398	0.84	0.380	1.68	0.380	1.40	0.400	3.50	0.396	14.0	0.370
0.84	0.370	1.96	0.360	3.50	0.360	3.50	0.382	7.00	0.378	28.0	0.358
1.96	0.352	2.80	0.352	5.60	0.350	7.00	0.364	14.0	0.358	56.0	0.346
2.80	0.346	4.20	0.346	11.20	0.340	14.0	0.348	28.0	0.340	112.0	0.334
4.20	0.340	5.60	0.342	14.00	0.338	21.0	0.340	42.0	0.334	168.0	0.330
5.60	0.340	7.00	0.340	19.60	0.336	35.0	0.332	49.0	0.332	280.0	0.326
θ (cm^2/mg)											
^{14}C		^{147}Pm		^{60}Co		^{137}Cs		^{36}Cl		^{90}Sr-^{90}Y	
0.57		0.930		2.14		5.65		9.90		20.70	

a 2π solid angle), $E(s)$, can be calculated by means of Eq. (5). Thus, we have

$$E(s) = f_T \int_0^{x_{\max}} \varepsilon_{ps}(x, \Delta, s) \Lambda_p(x) dx = f_T \Lambda \int_0^{x_{\max}} \varepsilon_{ps}(x, \Delta, s) f(x) dx \tag{14}$$

The efficiency of the large-area source is given by

$$\varepsilon(s) = \frac{E(s)}{f_T \Lambda} = \int_0^{x_{\max}} \varepsilon_{ps}(x, \Delta, s) f(x) dx \tag{15}$$

The transmission coefficient of beta particles emitted by the large-area source through the covering foil of thickness s is defined as the fraction of beta particles transmitted through this foil. As a result, we have

$$t(s) = \frac{E(s)}{E_S} = \frac{\varepsilon(s)}{\varepsilon_S} = \frac{\int_0^{x_{\max}} \varepsilon_{ps}(x, \Delta, s) f(x) dx}{\int_0^{x_{\max}} \varepsilon_{ps}(x, \Delta) f(x) dx} \tag{16}$$

One can be proved that $\varepsilon_{ps}(x, \Delta, s)$ from Eqs. (14), (15) and (16) must be replaced with $\varepsilon_p(x+s)$ if the covering foil, source substrate and backing plate are made from the same material. If only the covering foil and the source substrate are made from the same material, one can also be proved that $\varepsilon_{ps}(x, \Delta, s)$ from Eqs. (14), (15) and (16) must be replaced with $\varepsilon_p(x+s, \Delta+s)$.

5.2. Efficiency of large-area beta sources fabricated by the ink-jet printing technique

As an example of application, we calculate the efficiency of ^{36}Cl large-area reference sources fabricated by the ink-jet printing technique (Yamada et al., 2012). A thin layer of about 5 µm containing the radioactive material is applied by ink-jet printing technique on a substrate (polyester foil) of 0.1 mm thickness (14 mg/cm^2) which is mounted in an aluminum frame (4 mm thickness). To avoid radioactivity contamination, the source is covered with a 0.9 mg/cm^2 aluminized Mylar film. Because the effective atomic numbers of the polyester foil and the radioactive material are very close to the effective atomic number of the Mylar foil, we consider these materials as Mylar.

The source efficiency is calculated using Eq. (15), taking $x_{\max}$ = 0.7 mg/cm^2, s = 0.9 mg/cm^2, Δ = 14.7 mg/cm^2, assuming a homogeneous activity distribution ($f(x) = 1/x_{\max}$) and knowing that

$$\varepsilon_{ps}(x, \Delta, s) = \varepsilon_p(x+s, \Delta+s) = a_0 + a_1(x+s)^{0.5} + a_2(x+s) + a_3(x+s)^{1.5} + a_4(x+s)^2 + a_5(x+s)^{2.5}$$

The fitting parameters a_0, a_1, a_2, a_3, a_4 and a_5 were previously calculated at the end of the subchapter 2.3. Consequently, the calculated value of the source efficiency is 0.563. The experimental value of the source efficiency reported by Yamada et al. (2012) was 0.551. As one can see, there is a very good agreement between the experimental value and the calculated value of the source efficiency. This good agreement proves the usefulness of the plane source concept and the models developed for calculating the efficiency of large-area beta sources.

5.3. Detection efficiency of large-area detectors

For the sake of simplicity, we consider the planar geometry shown in Fig. 4 where the backing plate, the source substratum and the detector window are made from the same material. This geometry refers to the detection of beta particles using large-area detectors. The detection efficiency, $\varepsilon_{\det}$, is defined as the probability of detecting and recording beta particles by the counting system for a given counting geometry and detector (ICRU, 1994). As a result, we have

$$\varepsilon_{\det} = \frac{R}{f_T \Lambda} \tag{17}$$

where R is the count rate recorded by the counting system corrected for background, dead time losses and decay, Λ is the activity of the source. It is evident that

$$R = p_\beta E(s) \tag{18}$$

where p_β is the probability of detecting and recording of beta particles reaching the sensible volume of the detector and $E(s)$ is the rate of these particles. Knowing that $E(s) = t_w E_S = t_w f_T \varepsilon_S \Lambda$ (t_w is the transmission coefficient of beta particle through the detector window), it follows that

$$\varepsilon_{\det} = p_\beta \varepsilon_S t_w = \varepsilon_S \varepsilon_I \tag{19}$$

where $\varepsilon_I = p_\beta t_w$ is the instrument efficiency defined by ISO 7503-1. Using Eqs. (17), (18) and (14), we get

$$\varepsilon_{\det} = p_\beta \int_0^{x_{\max}} \varepsilon_p(x+s) f(x) dx = p_\beta \left[\varepsilon_p(s) - I(x_{\max}, s) \right] \tag{20}$$

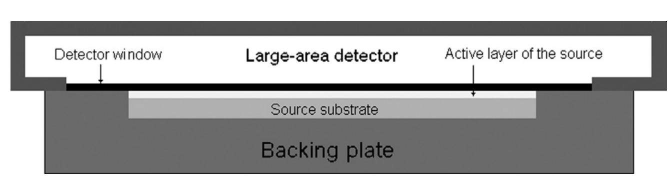

Fig. 4. Planar geometry for the detection of beta particles using large-area detectors.

where $I(x_{\max}, s) = \int_0^{x_{\max}} (\varepsilon_p(s) - \varepsilon_p(x+s)) f(x) dx$. As one can see from Eq. (20), the maximum value of the detection efficiency is $\varepsilon_{\text{det}}^{(\max)} = p_\beta \varepsilon_p(0) = 0.5 p_\beta (1 + \eta_S)$ obtained for $x_{\max}=0$ and $s=0$ (η_S is the saturation backscattering coefficient of the backing plate material). This means that the maximum of the detection efficiency is obtained by using windowless detectors and sources of negligible thickness deposited on materials having high atomic numbers (e.g. tungsten). It should be noted that $I(x_{\max}, s)$ is usually much smaller than $\varepsilon_p(s)$ (especially for high energy beta emitters such as ^{137}Cs, ^{36}Cl and ^{90}Sr-^{90}Y) for $s > x_{\max}$ which means that the detection efficiency depends weakly on $x_{\max}$ and *f(x)* under this condition. Consequently, surface contamination measurements are less susceptible to fluctuations of the contamination thickness and the depth activity distribution by using thick detector windows ($s > x_{\max}$) but the detection efficiency is significantly decreased in this case.

6. Conclusions

The modeling of the transmission of beta-rays through thin foils in planar geometry was performed using the plane source concept. The Pencyl code from the simulation package PENELOPE was used for computing the plane source efficiency and backscattering coefficients. Simple analytical expressions were obtained for the efficiency of plane sources and backscattering coefficients using least squares fitting of Monte Carlo data.

The utility of the modeling of the transmission of beta-rays through foils in planar geometry was proved in two applications regarding the efficiency of large-area beta sources and the detection efficiency of large-area detectors used for surface contamination measurements. Thus, the surface emission rate and the efficiency of large-area beta sources were defined by means of the plane source efficiency. It is shown that there is a simple relationship between surface emission rate of the source E_S and its activity Λ. As an example of application, the efficiency of large-area reference sources fabricated by the ink-jet printing technique was calculated. The detection efficiency of large-area detectors used for surface beta contamination measurements was also evaluated using the plane source concept. It is shown that the detection efficiency depends on the source efficiency and the transmission coefficient of beta radiation through the detector window. It is also shown that surface contamination measurements are less susceptible to fluctuations of the contamination thickness and the activity depth distribution by using thick detector windows.

Acknowledgments

This joint research project is financially supported by the European Commission in the frame of the European Metrology Research and Development Programme EMRP (http://www.emrponline.eu) undertaken by several EU Member States under the Article 169 initiative, JRP contract identifier EMRP ENV54 MetroDecom.

References

Baro, J., Sempau, J., Fernandez-Varea, J.M., Salvat, F., 1995. PENELOPE: an algorithm for Monte Carlo simulation of the penetration and energy loss of electrons and positrons in matter. Nucl. Instrum. Methods Phys. Res. B100, 31–46.

Bé, M.M., Chisté, V., Dulieu, C., Browne, E., Baglin, C., Chechev, V., Kuzmenko, N., Helmer, R., Kondev, F., MacMahon, D., Lee, K.B., 2006. Table of Radionuclides (Vol.3-A=3 to 244) Monographie BIPM-5 (2006) 98.

Berger, M.J., 1998. A method for determining the 2π-counting efficiency of beta-particle sources. Nucl. Instrum. Methods Phys .Res. B134, 276–286.

Berger, M.J., Unterweger, M.P., Hutchinson, J.M.R., 1996. The influence of backing and covering materials on the 2π-counting efficiencies of beta particles sources. Nucl. Instrum. Methods Phys. Res. A369, 684–688.

Haemers, S., Fredrikze, H., Wolterbeek, B. Th, 2007. A new approach to treat the attenuation of beta-rays in thin absorbers in planar geometry including covering foils. Nucl. Instrm. Methods Phys. Res. A 572, 768–773.

ICRU, 1994. ICRU Report 52: Particle Counting in Radioactivity Measurements, International Commission on Radiation Units and Measurements, Bethesda, Maryland.

IEC, 2002. Standard IEC 60325: Radiation Protection Instrumentation-Alpha, Beta and Alpha/Beta (Beta Energy > 60 keV) Contamination Meters and Monitors. International Electrotechnical Commission, Geneva.

ISO, 2010. Standard ISO 8769: Reference Sources for the Calibration of Surface Contamination Monitors-Beta Emitters (Maximum Beta Energy Greater than 0.15 MeV) and Alpha Emitters. International Organization for Standardization, Geneva.

ISO, 1988. Standard ISO 7503-1: Evaluation of Surface Contamination– Beta Emitters (Maximum Beta Energy Greater than 0.15 MeV) and Alpha-Emitters. International Organization for Standardization, Geneva.

ISO, 1996. Standard ISO 11932: Activity Measurements of Solid Materials Considered for Recycling, Re-use or Disposal as Non-radioactive Waste. International Organization for Standardization, Geneva.

ISO, 1992. Standard ISO 9697: WaterQuality—Measurement of Gross Beta Activity in Non Saline Water. International Organization for Standardization, Geneva.

Jansen, H., Klein, R., 1996. Characterization of large-area reference sources for the calibration of beta-contamination monitors. Nucl. Instrm. Methods Phys. Res. A 369, 552–556.

Pujol, Ll, Suarez-Navarro, J.A., 2004. Self-absorption correction for beta radioactivity measurements in water samples. Appl .Radiat. Isot. 60, 693–702.

Salvat, F., Fernandez-Varea, J.M., Sempau, J., 2003. PENELOPE—A Code System for Monte Carlo Simulation of Electron and Photon Transport. OECD Nuclear Energy Agency, Issy-les-Moulineaux, France.

Seliger, H.H., 1952. The backscattering of positrons and electrons. Phys. Rev. 88 (2), 408–412.

Sempau, J., Fernandez-Varea, J.M., Acosta, E., Salvat, F., 2003. Experimental benchmarks of the Monte Carlo code PENELOPE. Nucl. Instrum. Methods Phys .Res. B 207, 107–123.

Stanga, D., Maringer, F.J., Ionescu, E., 2011. A new method for determining the efficiency of large-area beta sources constructed from anodized aluminum foils. Appl. Radiat. Isot. 69 (1), 227–230.

Stanga, D., 2014. A simple method for determining the activity of large-area beta sources constructed from anodized aluminum foils. Appl. Radiat. Isot. 83, 211–215.

Svec, A., Janssen, H., Pernicka, L., Klein, R., 2006. A modified method for the characterization and activity determination of large-area sources. Appl. Radiat. Isot. 64, 1207–1210.

Vilches, M., Garcıa-Pareja, S., Guerrero, R., Anguiano, M., Lallena, A.M., 2007. Monte Carlo simulation of the electron transport through thin slabs: a comparative study of PENELOPE, GEANT3, GEANT4, EGSnrc and MCNPX. Nucl. Instrum. Methods Phys .Res. B 254, 219–230.

Yamada, T., Matsumoto, M., Yamamoto, S., Sato, Y., Yunoki, A., Hino, Y., 2012. Performance test and quality control of large area reference sources fabricated by the ink-jet printing technique. Appl. Radiat. Isot. 70 (9), 1964–1968.

Yunoki, A., Kawada, Y., Yamada, T., Unno, Y., Sato, Y., Hino, Y., 2013. Absorption and backscatter of internal conversion electrons in the measurements of surface contamination of ^{137}Cs. Appl. Radiat. Isot. 81, 261–267.